

Hot Jupiter Atmospheric Flows at High Resolution

Kristen Menou,^{1,2,3}

¹ *Physics & Astrophysics Group, Dept. of Physical & Environmental Sciences, University of Toronto Scarborough, 1265 Military Trail, Toronto, Ontario, M1C 1A4, Canada*

² *Dept. of Astronomy & Astrophysics, University of Toronto, 50 St. George Street, Toronto, Ontario, M5S 3H4, Canada*

³ *Dept. of Physics, University of Toronto, 60 St George Street, Toronto, Ontario, M5S 1A7, Canada*

Accepted XXX. Received YYY; in original form ZZZ

ABSTRACT

Global Circulation Models (GCMs) of atmospheric flows are now routinely used to interpret observational data on Hot Jupiters. Localized “equatorial β -plane” simulations by [Fromang et al. \(2016\)](#) have revealed that a barotropic (horizontal shear) instability of the equatorial jet appears at horizontal resolutions beyond those typically achieved in global models; this instability could limit wind speeds and lead to increased atmospheric variability. To address this possibility, we adapt the computationally efficient, pseudo-spectral PlaSim GCM, originally designed for Earth studies, to model Hot Jupiter atmospheric flows and validate it on the [Heng et al. \(2011\)](#) reference benchmark. We then present high resolution global models of HD209458b, with horizontal resolutions of T85 (128x256) and T127 (192x384). The barotropic instability phenomenology found in β -plane simulations is not reproduced in these global models, despite comparably high resolutions. Nevertheless, high resolution models do exhibit additional flow variability on long timescales (of order 100 planet days or more), which is absent from the lower resolution models. It manifests as a breakdown of north-south symmetry of the equatorial wind. From post-processing the atmospheric flows at various resolutions (assuming a cloud-free situation), we show that the stronger flow variability achieved at high resolution does not translate into noticeably stronger day-side infrared flux variability. More generally, our results suggest that high horizontal resolutions are not required to capture the key features of hot Jupiter atmospheric flows.

Key words: hydrodynamics – radiative transfer – planets and satellites: atmospheres – turbulence – astrochemistry – diffusion

1 INTRODUCTION

Hot Jupiters atmospheres have been extensively characterized by observational campaigns and, as a result, they provide some of the best laboratories available to us for studying the physics of exoplanet atmospheres [Charbonneau & Deming \(2007\)](#); [Seager & Deming \(2010\)](#); [Baraffe et al. \(2010\)](#); [Madhusudhan et al. \(2016\)](#); [Parmentier & Crossfield \(2018\)](#). The atmospheric flows that develop on these planets, with permanent day and night sides, are the subject of ongoing modelling efforts. While we know and have an understanding of what drives winds in these atmospheres ([Showman & Polvani 2011](#); [Hammond & Pierrehumbert 2018](#)), the dominant form of dissipation for wind kinetic energy is still the subject of intense debate. Indeed new physics is at play in these atmospheres: shocks ([Li & Goodman 2010](#); [Dobbs-Dixon & Agol 2013](#); [Fromang et al. 2016](#)) MHD effects ([Batygin & Stevenson 2010](#); [Perna et al. 2010](#); [Menou 2012](#); [Thorngren & Fortney 2018](#)) and vertical transport ([Menou](#)

[2019](#)) could all play a role in limiting the wind speeds on these planets.

In their study of shocks in hot Jupiter atmospheres, [Fromang et al. \(2016\)](#) found that a barotropic horizontal shear instability develops in a deep model of the specific hot Jupiter HD209458b. The phenomenology of this instability, and the time variable flow that results from it, is reminiscent of the barotropic instability discussed by [Menou & Rauscher \(2009\)](#) in their shallow hot Jupiter model (see also [Heng et al. 2011](#)). To this day, however, a similar shear instability has not manifested in any of the deep global hot Jupiter flow models published in the literature. [Fromang et al. \(2016\)](#) results suggest that this could be due to insufficient resolution in typical deep global model since the instability does not occur in their simulations until a demanding latitudinal resolution threshold is met (see their Figure 4). The existence of such an instability is important in (i) offering a novel avenue to limit wind speeds in hot Jupiter atmospheres and

(ii) in the possibility that it could manifest observationally in the form of atmospheric photometric and/or spectroscopic variability. Recently, [Komacek & Showman \(2019\)](#) have reviewed the observational evidence on hot Jupiter variability and presented a detailed exploration of the level of variability expected from global circulation models.

Here we reconsider the horizontal shear instability problem with PlaSim-Gen, an adaptation of the fast PlaSim Earth system simulator to the case of deep atmospheres such as those of hot Jupiters. Our work complements the recent study by [Komacek & Showman \(2019\)](#). The plan of this article is as follows. In §2, we describe our validation of the PlaSim-Gen model. In §3, we present high horizontal resolution models of HD209458b, which allow us to address the barotropic shear phenomenology of [Fromang et al. \(2016\)](#). We also present explicit post-processed day-side variability diagnostics of our atmospheric flow models. We find no corroborating evidence for the [Fromang et al. \(2016\)](#) phenomenology and establish that the flow variability exhibited in our high-resolution models does not translate into any significant additional observational variability in thermal emission. We conclude in §4.

2 PLASIM-GEN MODEL VALIDATION

As described in further details in Appendix A, PlaSim-Gen is an adaptation of PlaSim to model deep atmospheres such as those of hot Jupiters. In PlaSim-Gen, the atmosphere is decoupled from the surface, it is assumed dry and various Earth specific modules have been turned off. In the present version, the radiative forcing has been simplified by implementing Newtonian relaxation to precomputed radiative equilibrium profiles (see Appendix A for details).

We validate our implementation by reproducing the deep HD209458b benchmark of [Heng et al. \(2011\)](#). Our radiative relaxation profiles follow the polynomial fits of [Heng et al. \(2011\)](#). We perform the validation at a moderate resolution of T31L30, which is commensurate with other spectral-core models for hot Jupiters published in the literature (e.g. [Heng et al. 2011](#); [Rauscher & Menou 2012](#)). A model time step $\text{MPSTEP} = 180\text{s}$ and dissipation timescale $\text{TDISS} = 5 \times 10^{-3}$ were adopted. We run models up to 1200 planet days, which is longer than the typical runtime of models in the literature. Other model parameters are listed in Table 1 (see also Table A1 in Appendix A).

The top panels in Figure 1 and Figure 2 show, respectively, the zonal mean zonal wind profile and a representative horizontal temperature slice at the 260 mb level for our T31L30 validation model. We find that the outcomes from our validation model compare well to the reference results presented by [Heng et al. \(2011\)](#).

3 PLASIM-GEN HIGH RESOLUTION MODELS

Next, we move to high resolution versions of this HD209458b model. We focus on resolutions T85L30 and T127L30, which means that we increase the horizontal resolution while keeping the vertical resolution unchanged. This choice is dictated by our attempt to compare directly to the increased latitudinal resolution results discussed by [Fromang et al. \(2016\)](#). We

run our models with $\text{MPSTEP} = 60\text{s}$ (T85) and $\text{MPSTEP} = 45\text{s}$ (T127), and values of the hyperdissipation timescale applied to all dynamical variables $\text{TDISS} = 5 \times 10^{-4}$ (T85) and $\text{TDISS} = 1 \times 10^{-4}$ (T127). We find that PlaSim-Gen is fairly efficiently parallelized, up to 32 threads, allowing us to run a T127 model for 1200 planet days in less than a week of wall time on a modern workstation.

The middle panel in figures 1 and 2 show our T85L30 results while the lower panels show the T127L30 results. By and large, higher-resolution models reproduce the results of lower resolution versions (T31L30), with smaller-scale flow features that do not seem to impact much the global flow properties. This has already been noticed by [Heng et al. \(2011\)](#) and [Liu & Showman \(2013\)](#).

While the zonal wind structure, wind speeds and temperature maps are largely consistent across resolutions, careful examination reveals a deeper penetration depth of the equatorial jet and a somewhat larger north-south asymmetry (in both zonal wind and temperature maps), which seems absent from the lower T31L30 resolution runs.

These results are worth discussing in the context of the study of [Fromang et al. \(2016\)](#), who find a transition to a markedly different regime of circulation at latitudinal resolutions in excess of 64-128 cell elements (see their Figure 4). Our T85 and T127 runs do reach the latitudinal regime at which one might expect the dynamical transition witnessed by [Fromang et al. \(2016\)](#) to manifest. However, as exemplified in the lower two panels of Figure 2, even at high resolution, we do not find any evidence for the oscillatory/cyclic behavior of the equatorial regions reported by [Fromang et al. \(2016\)](#).

It is conceivable that our results on equatorial flow stability and lack of variability are sensitive to the level of hyperdissipation adopted in our models, as has already been discussed by [Heng et al. \(2011\)](#) for example. To address this possibility, we have run additional T31 and T85 models with different levels of hyperdissipation. We label T31_v1 and T85_v1 our previously described models with $\text{TDISS} = 5 \times 10^{-3}$ and 5×10^{-4} , respectively. We also ran models with higher levels of hyperdissipation: T31_v2 with $\text{TDISS} = 1 \times 10^{-3}$ and T85_v2 with $\text{TDISS} = 1 \times 10^{-4}$ (i.e., each with five times faster hyperdissipation than in v1 models). Overall we find little differences in atmospheric flow variability between v1 and v2 models.

To better quantify our various claims, we inspect the time viability of the equatorial wind speed at the 50mb level, which is one of the variability diagnostics studied by [Fromang et al. \(2016\)](#). Figure 3 shows planet-daily time-series of the equatorial zonal wind speed from planet day 100 to 1200 (avoiding transients from atmospheric spin-up in the first 100 planet days). There is little difference in the nature of the equatorial wind variability between the models with more or less hyper dissipation (at least at T31 or T85 resolutions).

There is however a noticeable difference in the nature of the variability in the high-resolution models (T85 and T127), relative to the moderate resolution models (T31). In particular, past 400 to 600 planet days, there are larger variations, ~ 10 to 20% in fractional amplitude, on timescales ~ 100 to 200 planet days, which are absent from the low resolution runs. While the emergence of this extra variability is intriguing in that it matches expectations in terms of the

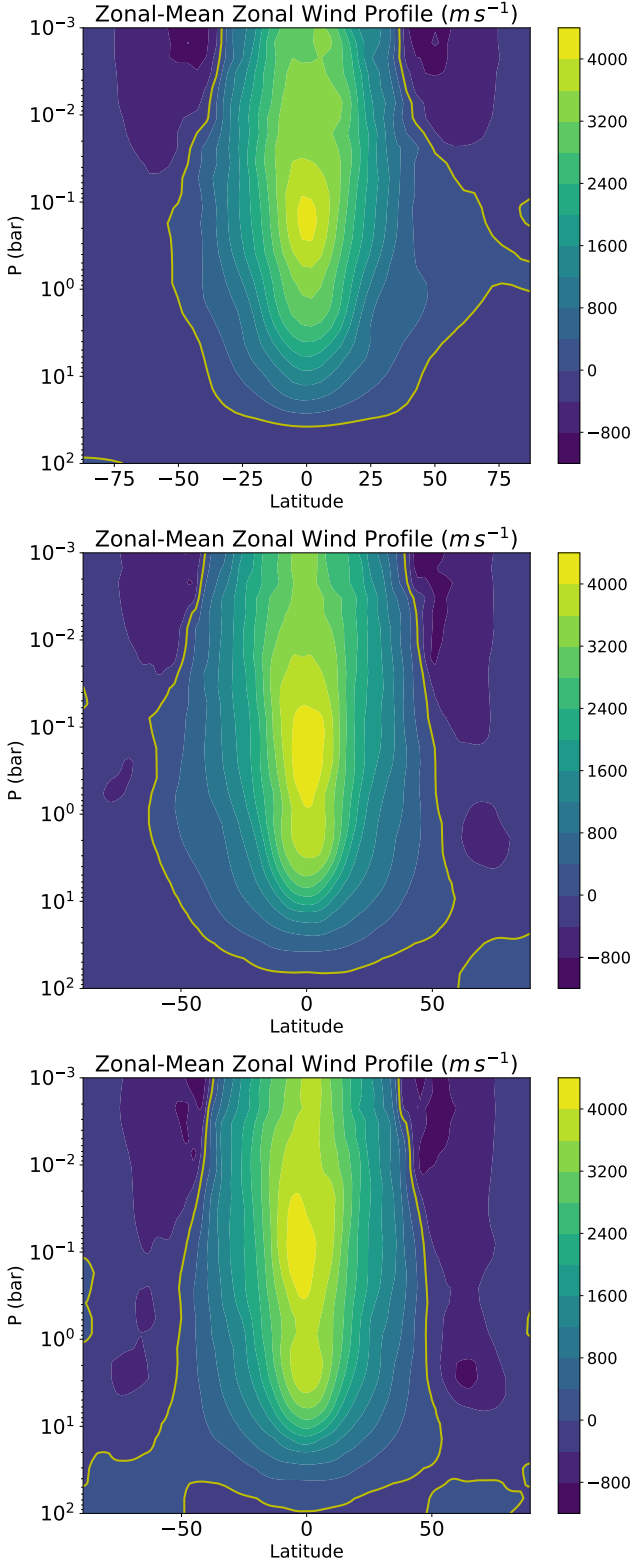


Figure 1. Zonally-averaged zonal wind profile at planet day 1200 in our T31L30 (top), T85L30 (middle) and T127L30 (bottom) models of HD209458b. Compare to Figure 12 in Heng et al. (2011).

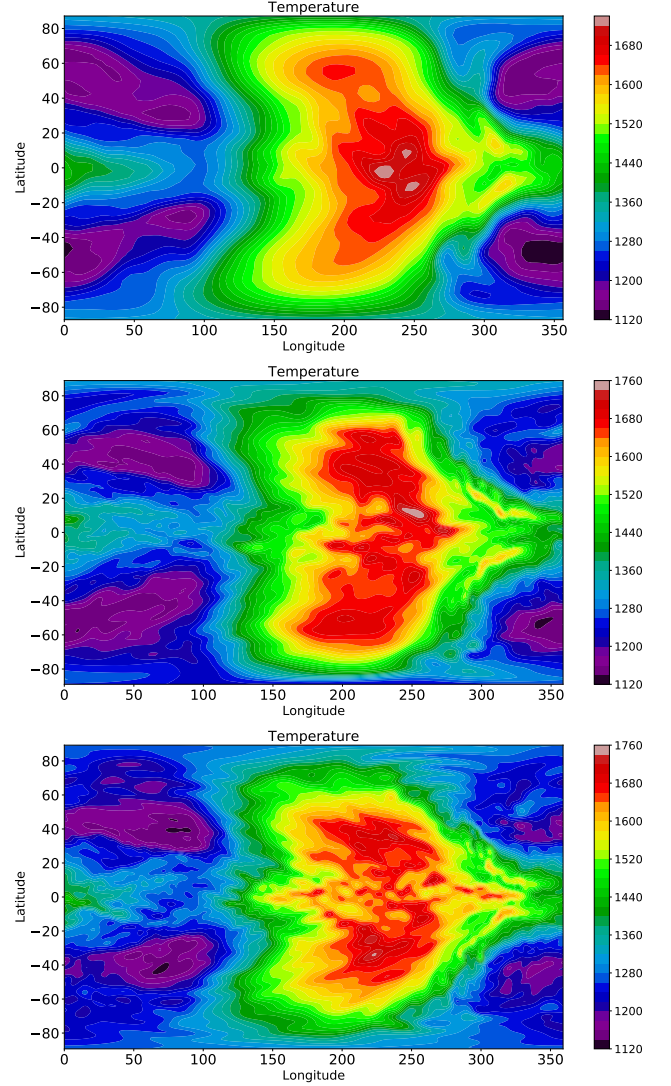


Figure 2. Temperature maps at the 260mb pressure level at planet day 1200 in our T31L30 (top), T85L30 (middle) and T127L30 (bottom) models of HD209458b. Compare to Figure 9 in Heng et al. (2011)

resolution requirements discussed by Fromang et al. (2016), we find that the phenomenology of this variability differs from that described by Fromang et al. (2016).

The significant shift in equatorial wind speeds, at the ~ 10 to 20% level, occur on much longer timescales in our high-resolution runs than the ones reported by Fromang et al. (2016) (\sim days). There is also no clear indication of wiggleness of the equatorial wind in our models (see Fig. 2). Furthermore, careful examination of our models reveals that the shifts in equatorial wind speed occur as a result of a minor, but noticeable, north-south breaking of symmetry in our high-resolution runs, which positions the peak wind speed somewhat above or below the equator. Some evidence for this behaviour is revealed in the lower two panels of Figures 1 and 2, although the effect is small.

One also notices in Figure 1 that the equatorial zonal flow reaches deeper in our T85, and even more so T127, mod-

els than in the T31 model. One possible interpretation for the overall phenomenology exhibited in our high-resolution models is that the atmospheric flow, driven from the top, eventually makes contact with the model lower boundary. This would happen at late times, past ~ 500 planet days, and more easily so in high resolution models, because these models better resolve the meridional circulation associated with the top-forced zonal flow and its gradual penetration with depth (see, e.g. [Showman et al. 2006](#)). We have not pursued this interpretation further since we believe that additional physical ingredients are needed first to adequately model the deep layers at pressures 10-100 bars and their interaction with the deeper planetary interior (see, e.g., the bottom drag included by [Liu & Showman 2013](#); [Komacek & Showman 2019](#)).

4 ATMOSPHERIC VARIABILITY

Variability in the atmospheric flow does not necessarily translate into observable photometric and/or spectroscopic variability. For example, small-scale variability may average out once the emission properties over an entire planetary hemisphere are considered.

To quantify the degree of photometric variability one might expect from the equatorial flow variability shown in Figure 3, we have post-processed our models T31_v1, T85_v1 and T127 with the petitRADTRANS open source tool [?]. As a diagnostic, we compute dayside emission in two separate narrow bands. We individually process each model column, weighting its emission by the cosine of the angle away from the substellar point, and then integrate all column contributions over the dayside hemisphere.

For concreteness, we adopt the same atmospheric composition parameters as the petitRADTRANS default code example (0.74 H₂, 0.24 He, 10^{-3} H₂O, 10^{-2} CO, 10^{-5} CO₂, 10^{-6} CH₄, 10^{-5} Na and 10^{-6} K, by mass). All other model parameters are chosen to match those our HD209458b model. The atmosphere is assumed to be cloud-free. To reduce the computational cost of processing from 16000 to 36000 dayside columns (for T85 and T127 resolutions, respectively), we focus on the emission in two representative narrow bands: 2.5-2.6 and 3.8-3.9 microns.

Figure 4 shows the dayside-integrated narrow-band photometric variability in these two bands (blue and orange solid lines), with the equatorial wind from Figure 3 superimposed as a green dash line. All quantities are shown in the time interval 800 to 1200 planet days and they have been normalized to emphasize relative variations. Comparing the top panel (T31_v1) to the lower two panels (T85_v1 and T127), it is clear that the larger equatorial wind variability (at the 10 to 20% level) in the high-resolution models does not translate into any significant additional variability in the two narrow infrared bands of interest, relative to the modest resolution model (top panel).

The dayside flux variations remain within the 2% variability level for all three models. This is consistent with our earlier observation that the larger equatorial wind variability at late times in the high-resolution models (Fig. 3) is largely caused by limited north-south shifts in the off-equatorial latitudinal location of the equatorial wind, which have limited

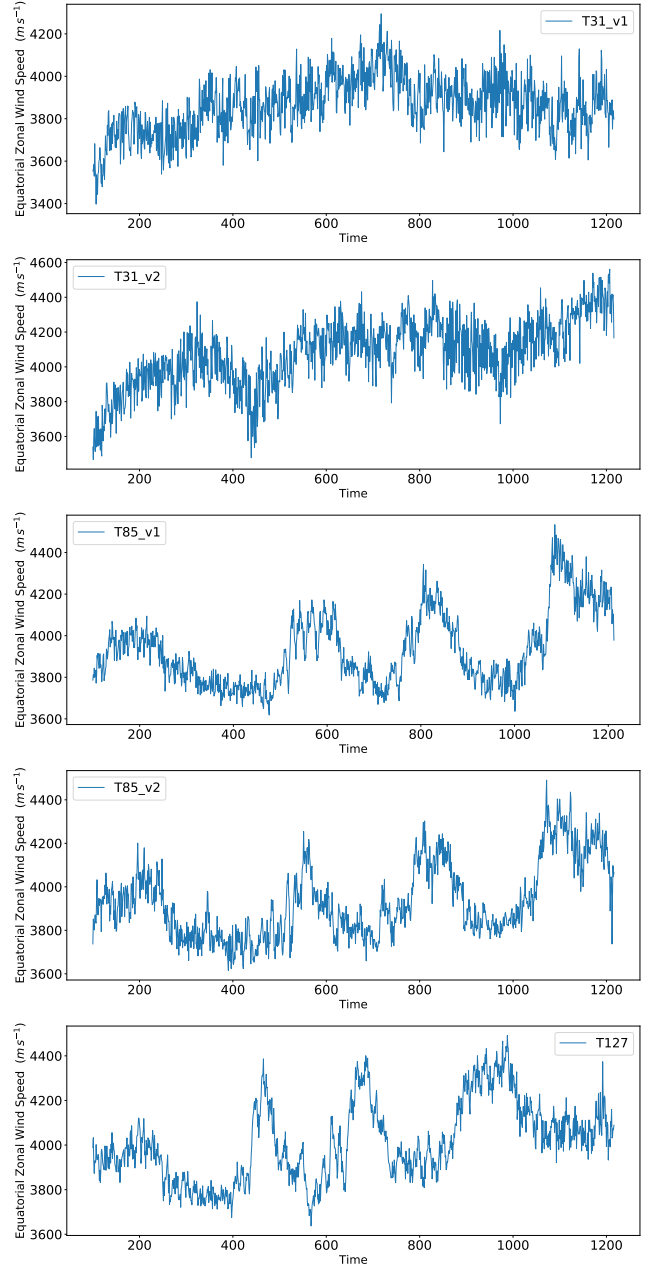


Figure 3. Equatorial zonal wind speed at the 53mb pressure level over planet days 100-1200. Compare to Figure 6 in [Fromang et al. \(2006\)](#).

impact on the dayside-averaged emission pattern of these atmospheres.

While not disproving the possibility of greater variability, e.g. when clouds are accounted for, our results illustrate well the point that atmospheric flow variability does not necessarily translate into a more readily observable photometric/spectroscopic variability.

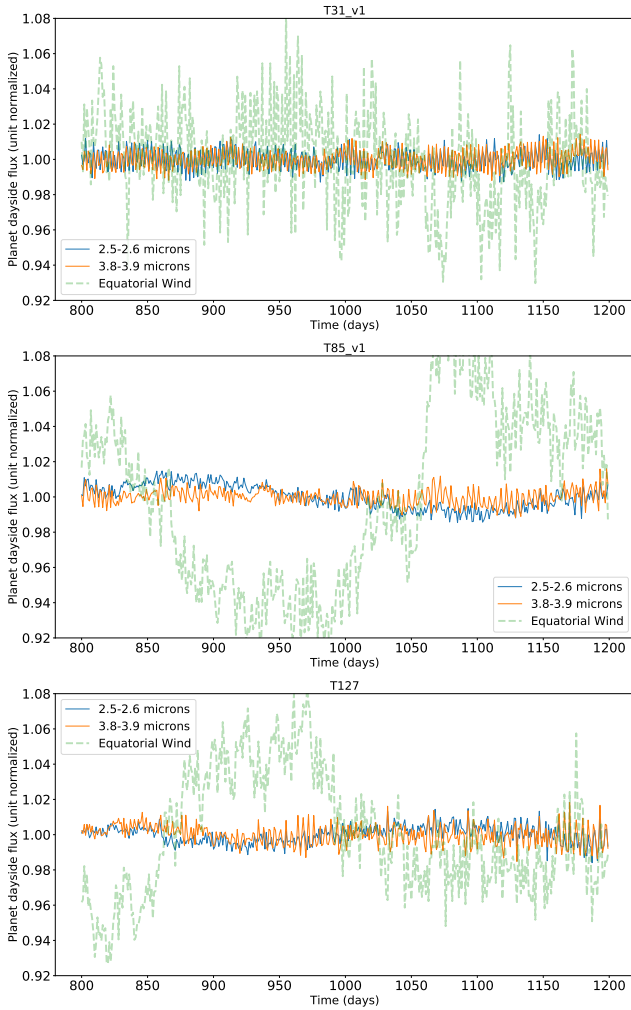


Figure 4. Variability over planet days 800-1200.

Table 1. Planet-Specific Model Parameters

Parameter	Value	Brief Description
GA	8	Gravitational acceleration (m/s^2)
SIDEREAL_DAY	285120.0	3.5 Earth day spin (s)
ECCEN	0	Planet eccentricity
OBLIQ	0	Planet obliquity
RADIUS	10^8	Planet Radius (m)
PSURF	10^7	Surface pressure (Pa)
OOM	5	Pressure range: $\log_{10}(PSURF/P_{top})$
AKAP	0.286	Ratio of gas constant to specific heat
GASCON	3523	Atmospheric gas constant
TGR	2700	'Ground' temperature (K)
SOLAR_DAY	285120.0	Solar day (s, unused)
GSOL0	1.06×10^6	Insolation flux (W/m^2 , unused)

5 DISCUSSION AND CONCLUSIONS

Superrotating equatorial jets like those realized in most simulations of hot Jupiter atmospheric flows are potentially subject to a barotropic (horizontal shear) instability (Kuo 1949; Vallis 2006). While the barotropic instability was triggered in the shallow hot Jupiter model of Menou & Rauscher

(2009), with $P_{bottom} = 1$ bar, none of the many deep hot Jupiter models ($P_{bottom} \geq 100$ bar) published to date have shown the barotropic instability phenomenology. In this context, the findings by Fromang et al. (2016) that a barotropically unstable hot Jupiter flow can indeed be achieved in their deep model ($P_{bottom} = 220$ bar), provided that the latitudinal resolution is high enough, are intriguing. Indeed, the reason why the barotropic instability did not manifest itself in other deep hot Jupiter models could simply be that these models did not have sufficient latitudinal resolution to resolve the instability onset.

To address this possibility explicitly, we have built models at horizontal resolutions well beyond those typically achieved in global models of hot Jupiter atmospheric flows. We have found that the barotropic instability does not manifest in our deep global models, even at high horizontal resolution. While the atmospheric flow exhibits increased variability at high resolution, and at late times, we associate this feature to the deeper penetration of the equatorial jet observed at higher resolution (see Figure 1) and not the barotropic instability.

Our findings raise a number of questions. First, while Mayne et al. (2017) and Mendonça (2019) have argued that very long integration times are needed to reach a balanced state in deep model layers for hot Jupiter conditions, our results suggest that the exact requirement may be resolution-dependent (see Figure 1) and perhaps model-dependent as well (e.g. spectral versus grid-based algorithm).

Second, the evidence so far suggests that shallow enough global models can be susceptible to the barotropic instability, while deep enough models are not (or at least less so, within current computational limitations). This could simply be the result of the greater challenge there is in maintaining a barotropic (vertically-aligned) flow across a larger number of pressure scale heights. In this respect, we note that the low-latitude flow is clearly barotropic (vertically aligned) over a greater vertical extent in our T127 model (lower panel of Figure 1), relative to the other two panels, but this is not enough to trigger a horizontal shear instability.

Third, the reason for the emergence of the barotropic instability in the deep models of Fromang et al. (2016) remains unclear at this point. It could be related to the β -plane approximation (which is only valid in the close proximity of the equator) or perhaps the compressible nature of the equations solved by Fromang et al. (2016), since compressible modes are filtered out from the hydrostatic equations solved in many published hot Jupiter models.

To conclude, it would seem that the use of only moderate horizontal resolutions in global hot Jupiter models is supported by our results, in the sense that high resolutions are not strictly necessary to capture the key features of the atmospheric flow. On the other hand, our results also highlight how a suitable approach to model the deep atmospheric layers and their coupling to the planetary interior is still missing and in need of physical clarification.

ACKNOWLEDGEMENTS

The author is grateful to Tad Komacek for comments on an early version of this manuscript. Computing resources were

provided by the Canadian Institute for Theoretical Astrophysics at the University of Toronto. KM is supported by the National Science and Engineering Research Council of Canada. This work has made extensive use of the following software packages: `matplotlib`, `petitRADTRANS`.

We would furthermore like to acknowledge that our work was performed on land traditionally inhabited by the Wendat, the Anishnaabeg, Haudenosaunee, Metis, and the Mississaugas of the New Credit First Nation.

REFERENCES

- Baraffe I., Chabrier G., Barman T., 2010, *Reports on Progress in Physics*, **73**, 016901
- Batygin K., Stevenson D. J., 2010, *ApJ*, **714**, L238
- Charbonneau D., Deming D., 2007, preprint, ([arXiv:0706.1047](https://arxiv.org/abs/0706.1047))
- Checlair J., Menou K., Abbot D. S., 2017, *ApJ*, **845**, 132
- Dobbs-Dixon I., Agol E., 2013, *MNRAS*, **435**, 3159
- Fraedrich K., Jansen H., Kirk E., Luksch U., Lunkeit F., 2005, *Meteorologische Zeitschrift*, **14**, 299
- Fromang S., Leconte J., Heng K., 2016, *A&A*, **591**, A144
- Hammond M., Pierrehumbert R. T., 2018, *ApJ*, **869**, 65
- Heng K., Menou K., Philipps P. J., 2011, *MNRAS*, **413**, 2380
- Komacek T. D., Showman A. P., 2019, arXiv e-prints, p. [arXiv:1910.09523](https://arxiv.org/abs/1910.09523)
- Kuo H.-L., 1949, *Journal of Atmospheric Sciences*, **6**, 105
- Li J., Goodman J., 2010, *ApJ*, **725**, 1146
- Liu B., Showman A. P., 2013, *ApJ*, **770**, 42
- Madhusudhan N., Agúndez M., Moses J. I., Hu Y., 2016, *Space Science Reviews*, **205**, 285
- Mayne N. J., et al., 2017, *A&A*, **604**, A79
- Mendonça J. M., 2019, arXiv e-prints, p. [arXiv:1910.10760](https://arxiv.org/abs/1910.10760)
- Menou K., 2012, *ApJ*, **745**, 138
- Menou K., 2019, *MNRAS*, **485**, L98
- Menou K., Rauscher E., 2009, *ApJ*, **700**, 887
- Paradise A., Menou K., 2017, *ApJ*, **848**, 33
- Paradise A., Menou K., Valencia D., Lee C., 2018, arXiv e-prints, p. [arXiv:1803.00511](https://arxiv.org/abs/1803.00511)
- Parmentier V., Crossfield I. J. M., 2018, *Exoplanet Phase Curves: Observations and Theory*. p. 116, [doi:10.1007/978-3-319-55333-7_116](https://doi.org/10.1007/978-3-319-55333-7_116)
- Perna R., Menou K., Rauscher E., 2010, *ApJ*, **719**, 1421
- Rauscher E., Menou K., 2012, *ApJ*, **750**, 96
- Seager S., Deming D., 2010, *Annual Review of Astron. & Astrop.*, **48**, 631
- Showman A. P., Polvani L. M., 2011, *ApJ*, **738**, 71
- Showman A. P., Gierasch P. J., Lian Y., 2006, *Icarus*, **182**, 513
- Thorngren D. P., Fortney J. J., 2018, *AJ*, **155**, 214
- Vallis G. K., 2006, *Atmospheric and Oceanic Fluid Dynamics*, [doi:10.2277/0521849691](https://doi.org/10.2277/0521849691).

APPENDIX A: PLASIM-GEN MODEL DESCRIPTION

PlaSim is an intermediate complexity Earth system simulator that is fast, parallelized, modular and extensively documented (Fraedrich et al. 2005). It has been used and extended before to study the climate of Earth-like exoplanets, with varying degrees of deviation from strict Earth conditions (e.g. Paradise & Menou 2017; Checlair et al. 2017; Paradise et al. 2018). Here we describe how we turned PlaSim into PlaSim-Gen, a generic simulator for deep atmospheres, by removing atmosphere-surface interactions and

implementing a simple Newtonian relaxation scheme to drive atmospheric motions.

Our first code-level modification is to redistribute model pressure levels on a logarithmic grid, starting at the bottom pressure level `PSURF` (a standard PlaSim parameter). We followed the exact same procedure as Rauscher & Menou (2012) in distributing sigma levels logarithmically over 00M orders of magnitude. Note that PlaSim’s dynamical core (PUMA) is a modern, parallelized version of the IGM spectral dynamical core used by Menou & Rauscher (2009); Rauscher & Menou (2012).

Our second code-level modification is to bypass PlaSim’s Earth-centric radiation scheme and directly implement, in the radiation module, temperature tendencies that obey a ‘Newtonian’ (linear) relaxation to a prescribed temperature profile, T_{eq} , on a prescribed radiative relaxation time, τ_{rad} :

$$\frac{\partial T}{\partial t} = \frac{T_{\text{eq}} - T}{\tau_{\text{rad}}}. \quad (\text{A1})$$

We adopt the fits of Heng et al. (2011) for the dayside and nightside profiles of T_{eq} and τ_{rad} , which makes our model specifically tailored to the hot Jupiter HD209458b.

Our third code-level modification is to change the timestep units in the code so that the parameter `MPSTEP` refers to the (integer) number of seconds per timestep (rather than minutes, as originally implemented). This is to accommodate the possibility of short timestep requirements when modeling hot atmospheres.

We have also removed a few Earth-specific prescriptions that were hardcoded in PlaSim (concerning the magnitude of horizontal hyperdissipation at specific resolutions)

Finally, we use the highly modular character of PlaSim to isolate relevant physics parametrizations while turning off all Earth-specifics, and otherwise unnecessary, modules. Table A1 lists the PlaSim parameter choices that allow us to model the deep atmosphere of the hot Jupiter HD209458b and to successfully benchmark against the similar implementation described in Heng et al. (2011).

In short, we select 30 vertical levels (spaced logarithmically), keep dry convective adjustment, choose an appropriate reference temperature and select a short enough timestep for numerical stability. We also adjusted the value of the Robert-Asselin time filter and the type of horizontal hyperdissipation implemented to be more in line with what has been used in other spectral dynamical cores when modeling hot Jupiters (e.g., Heng et al. 2011; Rauscher & Menou 2012). In terms of deselecting PlaSim modules, we turn off the sea ice and ocean modules, and we remove surface evaporation, surface fluxes and surface stresses. All precipitations are also turned off, so that our model is effectively dry with zero water content. We turned off PlaSim existing Newtonian relaxation scheme since it is super-seeded by the radiation scheme directly applied to temperature tendencies (Equation A1 above).

Note that some of our parameter choices are also chosen so that a suitable radiative transfer scheme would reproduce a tidally-locked hot Jupiter configuration (e.g. with the diurnal cycle on). Those choices are not strictly necessary given our hard-coding of temperature tendencies with a Newtonian relaxation scheme but they illustrate how PlaSim can

Table A1. PlaSim-Gen: Core Model Parameters

Parameter	PlaSim-Gen Value	Brief Description
NLEV	30	Number of (logarithmic) pressure levels
PNU	0.02	Robert-Asselin time filter
NDCA	1	Dry convective adjustment (on)
NPRL	0	Large scale precipitation (off)
NPRC	0	Convective precipitation (off)
NEVAP	0	Surface evaporation (off)
NPERPETUAL	1	Fixed Orbit (on)
NDCYCLE	1	Diurnal cycle (on)
NOCEAN	0	Ocean model (off)
NICE	0	Sea ice model (off)
NFLUX	0	Surface fluxes (off)
NSTRESS	0	Surface stresses (off)
NHDIFF	0	Cut off for horizontal diffusion (off)
MPSTEP	180	Seconds per timestep
T0	1400	Reference temperature (K)
TAUNC	0	Timescale for Newtonian cooling (off)

be extended to account for permanent dayside insolation with a full radiation scheme (as used in, e.g., [Checlair et al. 2017](#)).

This paper has been typeset from a $\text{\TeX}/\text{\LaTeX}$ file prepared by the author.